Crystal Structure of Diphtheria Toxin Bound to Nicotinamide Adenine Dinucleotide†

Charles E. Bell and David Eisenberg*

UCLA-DOE Laboratory of Structural Biology and Molecular Medicine, Molecular Biology Institute, and Department of Chemistry and Biochemistry, Box 951569, University of California at Los Angeles, Los Angeles, California 90095-1569

Received September 1, 1995; Revised Manuscript Received November 9, 1995⊗

ABSTRACT: Diphtheria toxin (DT), a 58 kDa protein secreted by lysogenic strains of *Corynebacterium diphtheriae*, causes the disease diphtheria in humans by gaining entry into the cytoplasm of cells and inhibiting protein synthesis. Specifically, the catalytic (C) domain of DT transfers the ADP-ribose group of NAD to elongation factor-2 (EF-2), rendering EF-2 inactive. In order to investigate how the C-domain of DT binds NAD and catalyzes the ADP-ribosylation of EF-2, the crystal structure of DT in complex with NAD has been determined to 2.3 Å resolution. This is the first crystal structure of an ADP-ribosyltransferase (ADP-RT) enzyme in complex with NAD and suggests the features of the ADP-RT fold which are important for NAD binding. The conformation of NAD in the complex and the proximity of the Glu148 carboxylate group of the C-domain to the scissile, N-glycosidic bond of NAD suggest plausible modes of catalysis of the ADP-ribosylation reaction. Residues 39−46 of the active-site loop of the C-domain become disordered upon NAD binding, suggesting a potential role for this loop in the recognition of the ADP-ribose acceptor substrate, EF-2. The negatively charged phosphates and two ribose hydroxyls of NAD are not in direct contact with any atoms of the C-domain. Instead, they form an exposed surface which appears to be presented for recognition by EF-2. Structural alignments of the DT−NAD complex with the structures of other members of the ADP-RT family suggest how NAD may bind to these other enzymes.

Nature commonly uses the enzymatic transfer of the ADP-ribose group of NAD[1] to a specific residue within a specific protein substrate (ADP-ribosylation) to regulate protein activity in both eukaryotic and prokaryotic cells. A subset of this large class of ADP-ribosyltransferase enzymes is a group of bacterial toxins that includes DT, cholera toxin (CT), pertussis toxin (PT), *Pseudomonas aeruginosa* exotoxin A (ETA), *Escherichia coli* heat-labile enterotoxins (LT), and several others (Passador & Iglewski, 1994; Burnette, 1994). Each of these bacterial toxins contains a domain which, upon entering the cytoplasm of mammalian cells, catalyzes the ADP-ribosylation of an acceptor residue within a specific target protein which ultimately results in either cell death or malfunction (Collier & Mekalanos, 1980; Moss & Vaughn, 1990). Although the crystal structures of four of these toxins, DT (Choe et al., 1992), ETA (Allured et al., 1986), LT (Sixma et al., 1991), and PT (Stein et al., 1994), have revealed a common fold within the bacterial toxin ADP-RT domains, in no case has the crystal structure of an ADP-RT enzyme in complex with NAD been reported.

DT was the first of the ADP-ribosylating toxins to be studied in detail, and over the course of several decades the basic mechanism by which DT elicits its cytocidal effect has been unraveled. DT consists of three structural domains which each carry out a distinct function in the killing process. The C-terminal receptor-binding (R) domain of DT (residues 385−455) binds to a cell surface receptor, permitting DT to enter a cell by the process of receptor-mediated endocytosis (Morris et al., 1985; Naglich & Eidels, 1990; Naglich et al., 1992). In the endosome, a drop in pH from ∼7 to ∼5 triggers a conformational change in the translocation (T) domain of DT (residues 201−384) which then inserts into the endosomal membrane and facilitates the transfer of the N-terminal, catalytic (C) domain (residues 1−191) across the endosomal membrane and into the cytoplasm (Sandvig et al., 1980; Moskaug et al., 1991; Blewitt et al., 1985). Once inside the cytoplasm, the C-domain of DT blocks protein synthesis (Collier, 1975) by catalyzing the transfer of an ADP-ribose group from NAD to a diphthamide (posttranslationally modified histidine) residue of EF-2 (Van Ness et al., 1980), forming a covalent bond between C1′N of NAD and the π-nitrogen atom of the imidazole ring of diphthamide. When the diphthamide residue of EF-2 is ADP-ribosylated, protein synthesis is inhibited and cell death occurs. The C-domain catalyzes this ADP-ribosylation reaction with essentially diffusion-limiting efficiency (K_{cat}/K_m approaching 10^{+8}; Blanke et al., 1994a), and it has been shown that a single C-domain of DT can kill a cell (Yamaizumi et al., 1978). In the absence of EF-2, the C-domain, as well as whole DT, catalyzes the slow hydrolysis of NAD at the N-glycosidic bond to ADP-ribose and nicotinamide, a reaction for which no biological significance has been demonstrated.

† This work was supported by NIH Grant GM31299 and USPHS National Research Service Award GM07185 (C.E.B.).

* Author to whom correspondence should be addressed.

⊗ Abstract published in *Advance ACS Abstracts,* January 1, 1996.

[1] Abbreviations: DT, diphtheria toxin; C-domain, catalytic domain of DT; T-domain, translocation domain of DT; R-domain, receptor-binding domain of DT; NAD, nicotinamide adenine dinucleotide; ApUp, adenylyl(3′−5′)uridine monophosphate; ADP-RT, adenosine 5′-diphosphate ribosyltransferase; NMN, nicotinamide mononucleotide; EF-2, elongation factor-2; ETA, *Pseudomonas aeruginosa* exotoxin A; PT, pertussis toxin; LT, *Escherichia coli* heat-labile enterotoxin; rms, root mean square.

0006-2960/96/0435-1137$12.00/0

Crystal structures of DT in complex with adenylyl(3′−5′)uridine monophosphate (ApUp) have previously been determined (Choe et al., 1992; Bennett et al., 1994; Bennett & Eisenberg, 1994; Weiss et al., 1995). Although this dinucleotide is bound to DT in preparations from *Corynebacterium diphtheriae*, the biological significance of ApUp remains uncertain. ApUp bears some molecular resemblance to NAD, and its binding site on DT has been assumed to mark the NAD-binding site. This site within the C-domain of DT is a prominent cleft between two subdomains. The side chains of His21 and Tyr65 lie within this cleft and have been shown by site-directed mutagenesis (Blanke et al., 1994a,b) and chemical modification studies (Papini et al., 1989, 1991) to be essential for NAD binding. UV cross-linking of the nicotinamide portion of NAD to the side chain of Glu148 (Carroll & Collier, 1984) and subsequent mutational studies at this site (Wilson et al., 1990) have revealed that the carboxylate group of Glu148 lies near the nicotinamide ring of NAD and is essential for catalysis of the ADP-ribosylation of EF-2. In order to determine more precisely how the C-domain of DT binds to NAD, and gain further insight into the mechanism by which the C-domain catalyzes the ADP-ribosylation of EF-2, we have determined the crystal structure of DT in complex with NAD to 2.3 Å resolution.

MATERIALS AND METHODS

DT Purification and Crystallization. DT was purified and dimerized as has been described (Carroll et al., 1986; Fujii et al., 1991) except that a chromatography step on DyeMatrex Gel Green A was added in order to separate the nucleotide-bound (predominantly ApUp) fraction of DT from the nucleotide-free fraction. The nucleotide-free DT fraction was collected and used for dimerization and crystallization. A 280/260 nm absorbance ratio of 1.7 measured for this DT sample verified that it was indeed nucleotide free. Nucleotide-free, dimeric DT was crystallized by the hanging drop vapor diffusion method at 22 °C, where the reservoir solution (1 mL) consisted of 12.0% PEG 8000 [poly(ethylene glycol) with an average molecular mass of 8 kDa], 0.43 M NaCl, and 0.043 M Tris buffer at pH = 7.5, and the hanging drop was prepared by adding 2 μL of 25 mg/mL dimeric DT in 50 mM Tris buffer, pH = 7.5, and 1 mM EDTA to 8 μL of 14% PEG 8000, 0.5 M NaCl, and 50 mM Tris buffer, pH = 7.5.

NAD Soaking, Flash-Freezing, and Data Collection. The problem of binding NAD, a hydrolyzable substrate, to DT, its enzyme, was solved as follows: over the course of 40 min, in microliter aliquots, 10 μL of a solution containing 19.7 mM β-NAD (Sigma), 14% PEG 8000, 0.5 M NaCl, and 0.05 M Tris at pH = 7.5 was added to an equilibrated hanging drop containing nucleotide-free DT crystals. This procedure resulted in the addition of a huge excess (>100: 1) of NAD over DT. After the final addition of NAD, a single crystal was transferred to 10 μL of a cryoprotectant solution containing 22.2 mM NAD, 18% PEG 8000, 0.5 M NaCl, 0.05 M Tris, pH = 7.5, and 20% glycerol. After 5 min the crystal was mounted in a hair loop (Teng, 1990) and immediately flash-frozen at −180 °C under a nitrogen vapor stream using an open-flow cryostat (Molecular Structure Corp.).

While the crystal was maintained at −180 °C, the reflection intensities were measured with a Rigaku R-Axis IIC imaging plate using a Rigaku RU-200 X-ray generator operating at 50 kV and 100 mA, equipped with a copper anode (λ = 1.54 Å) and Molecular Structure Corp. double focusing mirrors. All data were collected from a single crystal in 2.5°, 20-min oscillation images. At −180 °C, the radiation decay was so negligible that more than 100 20-min oscillation images were collected over the course of 2 days from a single crystal. The reflection intensities were integrated, merged, and scaled using the R-Axis II data processing software. Unit cell parameters and the quality of the intensity measurements are shown in Tables 1 and 2.

Table 1: Unit Cell Parameters for New Crystal Forms of DT

	nucleotide-free DT[a]	DT−NAD[b]
space group	*C*2	*C*2
a (Å)	105.2	105.0
b (Å)	91.2	89.5
c (Å)	65.3	130.1
β (deg)	94.1	94.0
no. of chains/au[c]	1	2

[a] Unit cell after soaking in cryoprotectant (18% PEG 800, 0.5 M NaCl, 0.05 M Tris buffer, pH = 7.5, and 20% glycerol) and flash-freezing at −180 °C. [b] Unit cell after addition of NAD and soaking in cryoprotectant (22.2 mM NAD, 18% PEG 8000, 0.5 M NaCl, 0.05 M Tris buffer, pH = 7.5, and 20% glycerol) and flash-freezing at −180 °C. [c] Number of DT molecules per asymmetric unit of the crystal.

Table 2: X-ray Intensity Measurements Collected for the NAD Complex of DT

no. of crystals	1
resolution	2.3 Å
no. of observations	157244
no. of unique reflections	49075
completeness	93.3% (87.4)[a]
R_{sym}[b]	7.7% (25.1)
$\langle I/\sigma \rangle$	9.0 (2.2)
B overall[c]	28.6 Å^2

[a] Numbers in parentheses refer to the 2.3−2.4 Å resolution data only. [b] $R_{sym} = 100\sum_h |I_h - \langle I \rangle| / \sum_h I_h$. [c] Overall temperature factor as estimated from a Wilson plot using data from 3.0 to 2.4 Å.

Molecular Replacement and Refinement. Molecular replacement and crystallographic refinement were performed using X-PLOR (Brünger, 1990). The initial starting model used for molecular replacement was the 2.0 Å structure of the dimeric DT−ApUp complex (Bennett et al., 1994b), with the ApUp and all water molecules removed. A self-rotation function gave no significant peaks other than the crystallographic 2-fold peak at $\psi = 0$, $\phi = 0$, and $\kappa = 180$. On the basis of this observation, it was considered likely that the DT dimer axis is coincident with the crystallographic 2-fold and that the asymmetric unit contains two half-dimers rather than one whole dimer. The cross-rotation function gave only one significant peak (9.1σ) at $\theta 1 = 180$, $\theta 2 = 0$, and $\theta 3 = 0$, indicating that each half-dimer in the asymmetric unit is in roughly the same orientation. After the PC-refined (Brünger, 1991) rotation was applied to the starting model, a translation function search gave a 10.0σ solution at x = 42.7 Å, y = 0 Å, z = 0 Å. After placement of the first half-dimer within the unit cell, a second translation search gave a 17.9σ solution at $x = -3.4$ Å, y = 9.1 Å, z = 65.2 Å, thus placing the second half-dimer within the unit cell.

All data ($I > 0\sigma$) from 8.0 to 2.4 Å were used for the first several rounds of refinement. The crystallographic *R*-factor after molecular replacement was 40.8%. After rigid body refinement, treating all six domains in the asymmetric unit as rigid bodies, the *R*-factor dropped to 38.2%. At this point 10% of the data were removed and placed into a test set in

Table 3: Refinement Statistics for the NAD Complex of DT

resolution	10.0−2.3 Å
R-factor[a]	22.7%
free *R*-factor[b]	30.7%
no. of atoms (non-hydrogen)	
total	8295
protein	7905
NAD	88
water	302
rms deviations from ideal geometry	
bonds	0.013 Å
angles	1.7°
dihedrals	25.2°
impropers	1.5°
mean temperature factors (Å^2)	
all atoms	26.3
protein atoms	26.5
NAD atoms	29.3
solvent atoms	20.3[c]

[a] $R = 100\sum_h||F_o| - |F_c||/\sum_h|F_o|$. [b] Free *R*-factor is calculated for 10% of the data which were omitted from the refinement. [c] Several of the solvent temperature factors refined to unusually low values and were restricted to a minimum value of 10.0.

order to monitor the free *R*-factor, which was 37.8% after rigid body refinement. In all subsequent refinement procedures, the free *R*-factor (Brünger, 1992) was used to protect against overfitting, until the final stages of refinement where the reflections from the test set were added back to the working set. During the first and all subsequent rounds of refinement, which included simulated annealing (Brünger et al., 1990) and restrained isotropic temperature factor refinement, noncrystallographic symmetry (ncs) restraints were imposed except in regions of each half-dimer lying in different environments due to crystal packing; these were not restrained. During early rounds of refinement an ncs weight of 300 was used and dropped down to 50 for the final round. After the first round of refinement the *R*-factor and free *R*-factor dropped to 27.4% and 34.4%, respectively. The model was then manually refit to annealed omit maps (Hodel et al., 1992) using FRODO (Jones, 1978) on an Evans and Sutherland graphics workstation. After several more rounds of crystallographic refinement and manual refitting, combined with the addition of 248 water molecules and two NAD molecules, the *R*-factor and free *R*-factor were 22.3% and 30.9% respectively. At this point, data from 10.0−8.0 Å, 2.4−2.3 Å, and the test set were added to the refinement, and further rounds of model building, addition of water molecules, and crystallographic refinement were performed.

The quality of the final model is shown in Table 3. The final model consists of all residues of both half-dimers in the asymmetric unit except for residues 39−46 of the C-domain and residues 188−199 of the loop between the C- and T-domains. These residues were not included in the model for either of the two half-dimers in the asymmetric unit because suitable electron density was not observed, presumably due to disorder. The rms deviation between the two half-dimers in the asymmetric unit is 0.11 Å. The ϕ, ψ torsion angles for 91.0% of the residues are within the most favored regions of the Ramachandran plot, as defined by Morris et al. (1992). Only one residue, AspB465, has ϕ, ψ torsion angles in the disallowed region of the Ramachandran plot. This residue is in a surface loop for which the temperature factors are high (∼80 Å^2).

The atomic coordinates and structure factors for the structure of the DT−NAD complex have been deposited in the Brookhaven Protein Data Bank (identification code 1TOX).

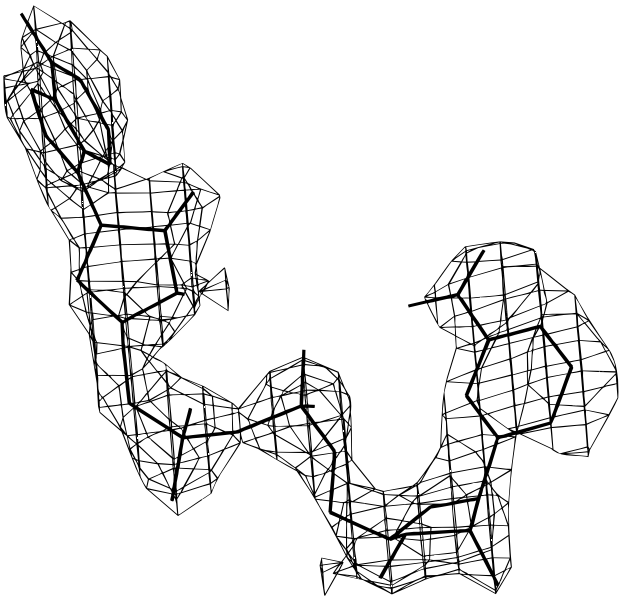

FIGURE 1: Electron density for NAD in the DT−NAD complex. The $2F_o - F_c$ electron density is shown for NAD at 2.4 Å resolution contoured at 1σ for one of the DT molecules in the asymmetric unit. The electron density map (thin lines) is shown superimposed on the final, refined NAD molecule (thick lines). The map was calculated before NAD was included in the refinement (when R = 23.8%) and is therefore unbiased. The electron density for the other NAD molecule in the asymmetric unit is of comparable quality. The figure was prepared using FRODO (Jones, 1978).

RESULTS

Preparation of the DT−NAD Complex. The low affinity of DT for NAD (K_d ∼10^{-5} M; Lory et al., 1980), combined with the DT-catalyzed hydrolysis of NAD at the N-glycosidic bond (Lory et al., 1980), has been a significant obstacle in determining the structure of DT in complex with NAD, as has been the case (to an even greater extent) with other ADP-RT enzymes. Our first attempt to overcome this problem was to use carba-NAD (Slama et al., 1988), a nonhydrolyzable analog of NAD which has carbon substituted for O5′N. Although we were able to grow crystals of dimeric DT in the presence of carba-NAD and collect several data sets to 2.5 Å resolution, interpretable density for this analog in the active-site region of the C-domain was never observed, even at very high concentrations of carba-NAD. Subsequent assays by fluorescence quenching revealed that carba-NAD binds to DT significantly less tightly than does NAD (data not shown).

This led us to try a "soak/freeze" experiment in which (1) crystals of nucleotide-free DT were grown, (2) the crystals were soaked with a huge excess of NAD, and then (3) the solution was transferred to a cryoprotectant and immediately flash-frozen at −180 °C in order to prevent NAD hydrolysis. Although in our initial experiments the crystals cracked upon the addition of NAD, we found that, by adding the NAD gradually in the presence of higher PEG 8000 concentrations, we were able to prepare (after several trials) an NAD-soaked crystal which was suitable for measurement of the X-ray reflection intensities to 2.3 Å resolution.

The addition of NAD to nucleotide-free DT crystals altered the crystal packing such that the unit cell doubled in volume (see the *c* axial lengths in Table 1). This immediately

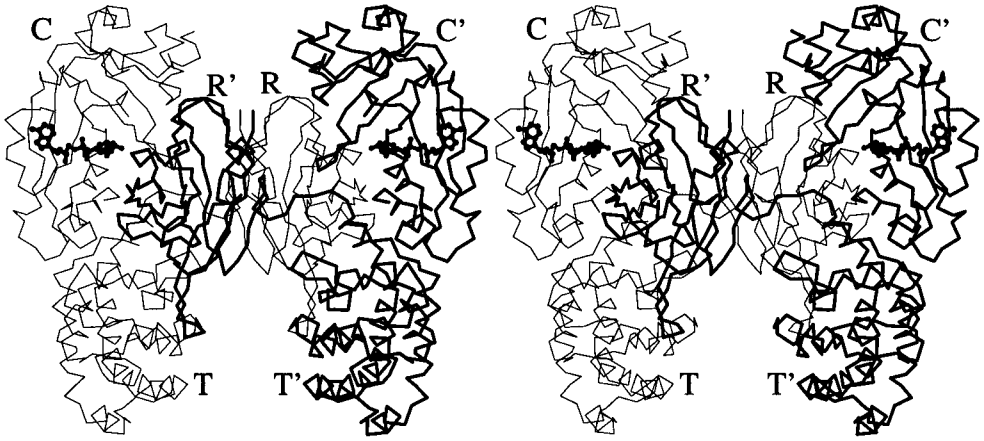

FIGURE 2: Stereo Cα trace of the DT dimer bound to NAD. One subunit of the dimer is shown in thin lines and the other subunit in thick lines. The receptor-binding, translocation, and catalytic domains are labeled R, T, and C for one subunit and R′, T′, and C′ for the other subunit. The two NAD molecules are shown in ball-and-stick form. The molecular dyad is vertical and in the plane of the paper. This figure and Figures 3, 4, 6, 8, and 9 were prepared using MOLSCRIPT (Kraulis, 1991).

suggested that some significant structural change occurs in DT upon NAD binding. In addition, since the nucleotide-free DT dimer crystal is isomorphous with the DT−ApUp dimer crystal [see Table 1 and Bennett et al. (1994)], the change in unit cell suggested further that the structural change induced by NAD binding is not as simple as an "open" and "closed" conformation for the nucleotide-free and nucleotide-bound states, respectively.

The structure of the DT−NAD complex was determined as detailed in Materials and Methods. After refinement, a $2F_o - F_c$ electron density map contoured at 1σ (Figure 1) showed clear, readily interpretable density for NAD in the active sites of both of the DT molecules in the asymmetric unit.

Overall Description of the DT Dimer−NAD Complex. In Figure 2, a stereo diagram of the dimeric DT−NAD complex shows the R-, T-, and C-domains of DT. The dimer is "domain swapped" (Bennett et al., 1994a): the R-domains of the two subunits are exchanged, forming extensive contacts with the C- and T-domains of the other subunit of the dimer. NAD binds to a cleft on the surface of each C-domain of the dimer, very near to the interface with the R-domain. Overall, the structure of the dimeric DT−NAD complex is very similar to that of the dimeric DT−ApUp complex. There are no major differences in the relative positions of the R-, T-, and C-domains in the two structures. In the dimeric DT−NAD crystal, the molecular dyad is coincident with the crystallographic 2-fold along the *b*-axis. The asymmetric unit contains two half-dimers that are related by a translation. There are no major differences in the structures of the two half-dimers in the asymmetric unit. Minor differences occur at regions where different crystal contacts are formed.

Overall Binding of NAD to DT. As shown in the ribbon representation of the C-domain−NAD complex in Figure 3 (the R- and T-domains have been omitted in the figure, although they are present in the structure), NAD binds to a prominent cleft on the front face of the C-domain, in approximately the same position as ApUp (Figure 4a). This cleft is formed at the junction of the two approximately orthogonal, antiparallel β-sheet subdomains. Both the overall fold of the C-domain and the NAD-binding site are quite distinct from (and unrelated to) the Rossmann fold of several dehydrogenase enzymes (Rossmann et al., 1975) in which the NAD-binding site is at the carboxy terminus of a parallel

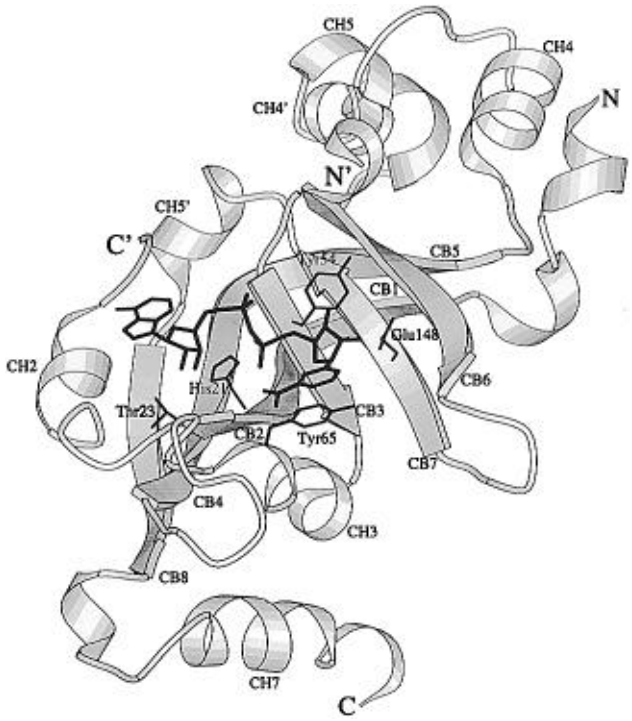

FIGURE 3: Ribbon representation of the C-domain of DT bound to NAD. The C-domain is shown in gray and NAD is shown in black in stick form. The side chains of Glu148, His21, Tyr54, Tyr65, and Thr23 are also shown in black in stick form. Only the C-domain of DT is shown; the R- and T-domains have been omitted from the figure even though they are present in the crystal structure. Residues 39−46 are not included in the model for the C-domain. Residue 1 is labeled N, residue 187 is labeled C, residue 38 is labeled C′, and residue 47 is labeled N′. β-Sheets are labeled CB1−CB8, and α-helices are labeled CH2-CH7, according to Bennett et al. (1994b).

β-sheet. Residues of the C-domain which line the inside of this cleft and make direct contacts with NAD extend primarily from the following secondary structural elements: CB2, CH2, CB3, and CH3 [secondary structures labeled as in Bennett et al. (1994b)].

As can be seen in the structural alignment of the DT−ApUp and DT−NAD complexes shown in Figure 4a, although NAD and ApUp bind to approximately the same position within the active-site cleft, all of the individual components of each of these dinucleotides (with the exception of the adenine rings) are in significantly different

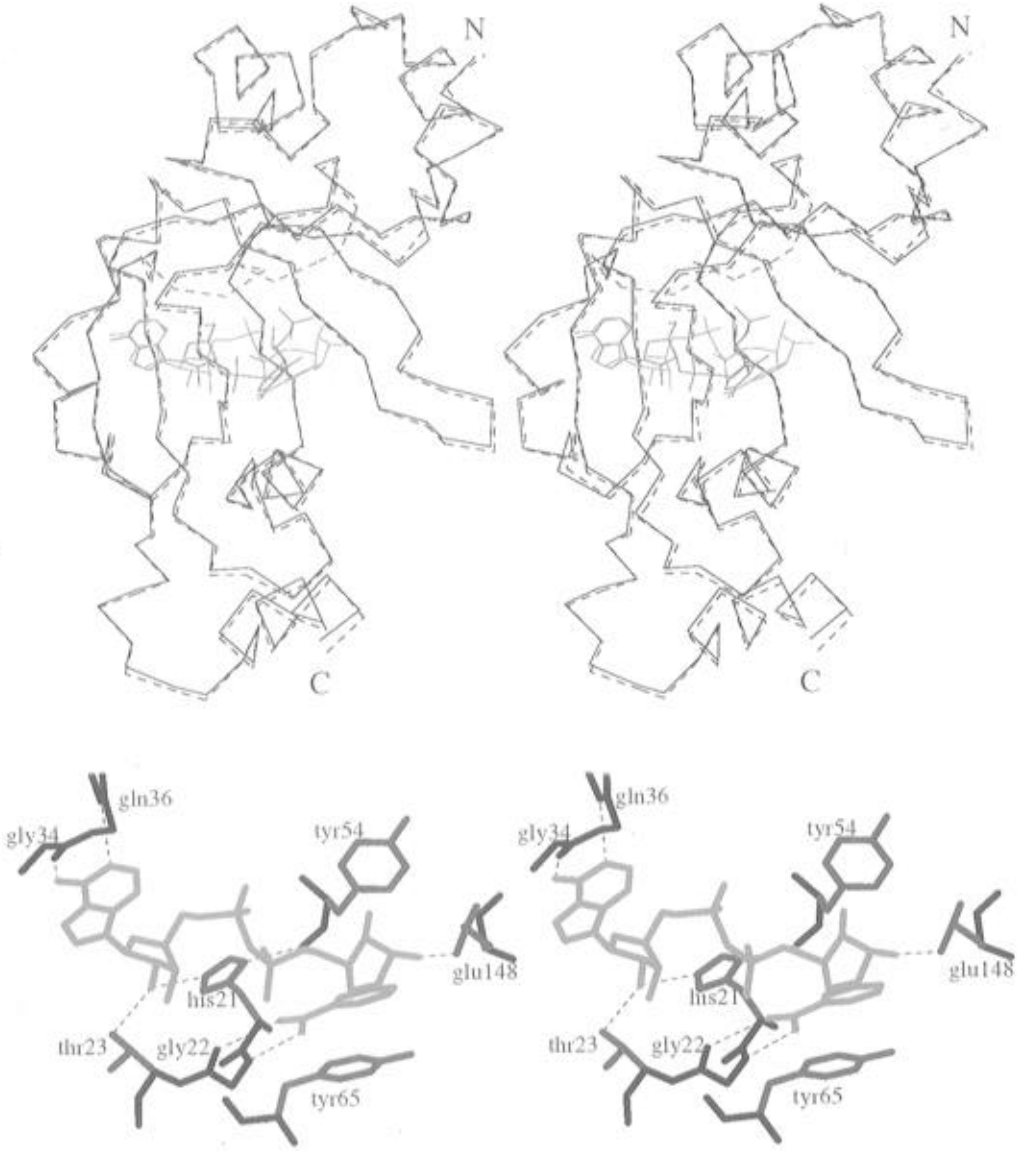

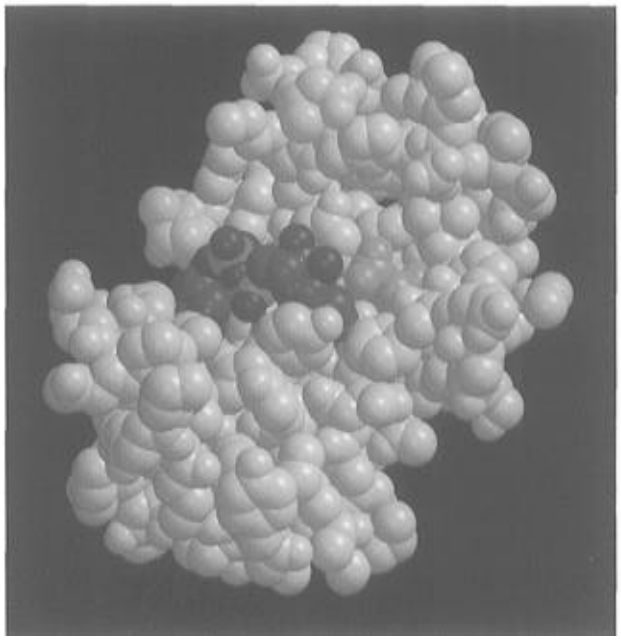

FIGURE 4: (a, top) Stereoview comparing the C-domain of DT when complexed to either ApUp or NAD. The structure of the C-domain−NAD complex is shown as a Cα trace in solid black lines with NAD in blue. The structure of the C-domain−ApUp complex is shown as a Cα trace in black dashed lines with ApUp in green. The active-site loop residues 39−47 of DT in complex with ApUp are highlighted in red. These residues are not observed in the structure of the complex between DT and NAD. The structures of the two complexes are superimposed on the basis of an alignment of the protein structures. The view is in approximately the same orientation as in Figure 3. (b, middle) Stereoview of the atomic interactions between the C-domain of DT and NAD. NAD is shown in blue, backbone atoms are in black, and side-chain atoms are in red. Hydrogen bonds are shown as dashed lines. Two water molecules, which make several hydrogen bonds to NAD and the C-domain, have been omitted for clarity. The view is in approximately the same orientation as in Figure 3 and part a of this figure. (c, bottom) Space-filling diagram of the C-domain of DT in complex with NAD to illustrate the exposed surface of NAD in the complex. Only those atoms of the C-domain within 15 Å of NAD are shown. Atoms of the C-domain are shown in gray with the exception of the active-site residue Glu148 (light blue) and the two residues at the ends of the active-site loop, Pro38 and Asp47 (yellow). Residues 39−46 are not seen in the structure. Carbon atoms of NAD are shown in red, oxygen atoms in blue, and phosphorus atoms in green. The exposed surface of NAD includes the negatively charged phosphates (blue and green), which provide the potential for electrostatic interactions with EF-2, and the NMN ribose hydroxyls (blue), which provide the opportunity for hydrogen-bonding interactions with EF-2.

positions such that most of the specific contacts between the C-domain and each of these dinucleotides are different. One significant difference is in the contribution of the R-domain to substrate binding. In the DT−ApUp complex, residues Arg458 and Ser446 of the R-domain make direct contacts to the phosphates of ApUp. In the DT−NAD complex, the two phosphates of NAD are in significantly different positions compared to the two phosphates of ApUp in the DT−ApUp complex (see Figure 4a). Consequently, Arg458 and Ser446 of the R-domain are not within hydrogen-bonding or salt-bridge distance of NAD, as they are in the DT−ApUp complex.

Structural Changes in DT upon NAD Binding. Upon the addition of NAD to nucleotide free DT crystals, the unit cell dimensions change (see Table 1), suggesting that some significant structural change occurs in DT upon NAD binding. The change in unit cell that occurs is not a result of higher PEG 8000 concentrations (16% used during NAD soaking, 18% used as cryoprotectant) because the nucleotide-free crystal does not exhibit this change in unit cell upon soaking in cryoprotectant solution containing 18% PEG 8000 (see Table 1). Overall, as seen in Figure 4a, the structure of the C-domain when bound to NAD is virtually identical to the C-domain when bound to ApUp (the two structures can be superimposed to an rms deviation of 0.3 Å for all atoms). There is no significant movement of the two subdomains of the C-domain relative to one another.

The part of the C-domain structure that does change when NAD is added is residues 39−46 of the loop between CH2 and CB3 (see Figures 3 and 4a), which we have termed the "active-site" loop. In the DT−NAD structure, these residues are not visible in the electron density maps for either of the two molecules in the asymmetric unit and thus are presumed to be disordered and have been excluded from the model. In all three previous structures of the C-domain in complex with ApUp [DT monomer (Bennett & Eisenberg, 1994), DT dimer (Choe et al., 1992; Bennett et al., 1994b), and isolated C-domain (Weiss et al., 1995)], these residues form a loop that is well ordered and extends out over the active-site cleft making contacts with ApUp. In the structure of nucleotide-free DT (Bell and Eisenberg, unpublished results), these residues are also well ordered and in approximately the same position as in the DT−ApUp complex. In the DT−ApUp and nucleotide-free DT crystals, which are isomorphous, this loop makes all of the crystal contacts in the *c*-direction. Thus, a disruption of this loop is responsible for the change in unit cell that occurs upon the addition of NAD to nucleotide-free DT crystals (see Table 1).

It is not apparent why NAD binding to DT causes residues 39−46 of the active-site loop to become disordered. An alignment of the DT−ApUp structure (or nucleotide-free DT) with the DT−NAD structure (Figure 4a) shows that although NAD binds within 3.5 Å of the position of the active-site loop in DT−ApUp (and in nucleotide-free DT), there is no direct overlap, and thus NAD binding to the C-domain would not directly sterically displace the active-site loop. The displacement of the active-site loop cannot be explained by electrostatic repulsion with the negatively charged phosphates of NAD, as there are no negatively charged residues in this loop that lie near the phosphate-binding site. In addition, the temperature factors of the protein do not suggest disorder in the region surrounding this loop. Therefore, although we observe that NAD binding to DT induces a structural change in the active-site loop, resulting in a disruption of crystal

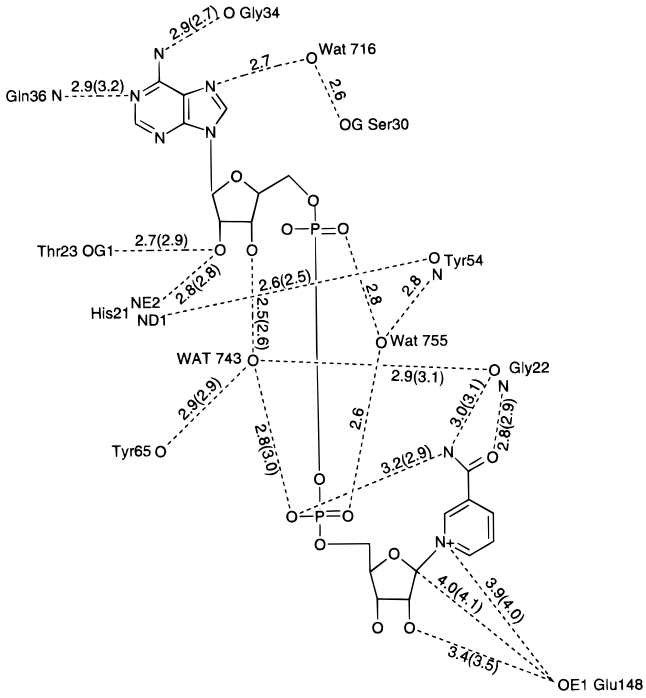

FIGURE 5: Distances between atoms of the C-domain of DT and NAD. Distances for the second molecule in the asymmetric unit are shown in parentheses. All dashed lines represent hydrogen bonds with the exception of those from Glu148 OE1 to N1N and C1′N, which are relevant to catalysis.

contacts, at present we have no explanation for why this change occurs. As discussed below, the observation that this loop changes structure upon NAD binding suggests that these residues may be important for binding to the ADP-ribose acceptor substrate EF-2.

Conformation of Bound NAD. This is the first crystal structure of an enzyme bound to NAD in which the NAD is utilized as a labile substrate rather than as a cofactor for electron transfer. The conformation of NAD when bound to DT, viewed in Figures 1, 3, and 4, differs substantially from that of NAD when bound to several oxidoreductase enzymes having the Rossmann fold, reflecting this difference in function. The adenine ring of NAD in the complex is in the unfavorable syn ($\chi = -80°$) conformation with a ribose pucker of C2′-endo. The γ-dihedral angle (O5′−C5′−C4′−C3′) is at 95°, resulting in the usual open, extended conformation for the AMP portion of NAD. In contrast, the NMN moiety is in a closed conformation with γ at −60°. The nicotinamide is in the syn conformation ($\chi = 0°$) with a ribose pucker of C3′-endo. This results in a highly folded, compact structure for the NMN portion of NAD, where a hydrogen bond is formed between N7 of the carboxamide group and O3P of the NMN phosphate. The C1′N atom of NAD, which reacts with the diphthamide residue of EF-2 in the ADP-ribosylation reaction, faces away from the active-site pocket and is exposed to solvent (see Figure 4c).

Atomic Contacts between DT and NAD. Figures 4b and 5 show the atomic interactions between the C-domain and NAD. NAD forms roughly a U-shape such that the adenine and nicotinamide rings at each end of the U project into the active-site cleft of the C-domain, making extensive hydrophobic and hydrogen-bonding interactions, while the phosphates at the base of the U stick out of the cleft and are more exposed to solvent. This is shown in the space-filling model of the C-domain−NAD structure in Figure 4c. The adenine and nicotinamide rings of NAD each make a pair

of hydrogen bonds to each of two backbone segments of the C-domain around glycine residues. The adenine N7A and N1A atoms hydrogen bond to Gly34 O and Gln36 N, respectively, and the N7N and O7N atoms of the carboxamide group of nicotinamide hydrogen bond to Gly22 O and N, respectively. These pairs of hydrogen bonds may help to keep the orientation of the adenine and nicotinamide rings fixed, where the glycine residues would give the backbone extra flexibility needed to make tight pairs of hydrogen bonds with each of the bases.

Adenine and nicotinamide also make extensive hydrophobic contacts with residues of the C-domain within the active-site cleft. While the adenine ring binds in a hydrophobic pocket formed by Trp153, Pro38, Tyr27, Ile31, Ile35, and Phe53, the nicotinamide ring and the NMN ribose fit into a groove formed by Tyr54 and Tyr65. Although the nicotinamide ring of NAD is 4 Å above and parallel to the phenyl ring of Tyr65, the two six-membered π-electron systems are not stacked directly on top of one another.

The carboxylate group of Glu148, a residue which has been shown to be critical for catalysis of the ADP-ribosylation of EF-2, is 4 Å from the N1N and C1′N atoms of NAD which form the scissile, N-glycosidic bond. On the basis of this distance, the potential role of Glu148 in catalysis of the ADP-ribosylation of EF-2 will be discussed below.

The phosphate and ribose groups of NAD make far fewer interactions with the C-domain than do the bases and are mostly solvent exposed (see Figure 4c). O2′A of the adenosine ribose hydrogen bonds to Thr23 OG1 and to His21 NE2. Surprisingly, the negatively charged phosphates of NAD make no direct contacts to the C-domain and are not neutralized by nearby positive charges of the protein. The phosphates do, however, make indirect hydrogen bonds to the backbone carbonyl oxygen atoms of Tyr65, Tyr54, and Gly22, through two well-ordered water molecules. The two water molecules each make additional hydrogen bonds to NAD (see Figure 5) and thus appear to be important for stabilizing the active-site pocket. The NMN ribose hydroxyls, together with the negatively charged phosphates, form an exposed surface of NAD (see Figure 4c) which could potentially be important for binding to EF-2, as will be discussed below.

Trp50, a residue that is conserved in DT and ETA, has been shown by site-directed mutagenesis to be a major determinant of NAD affinity (Wilson et al., 1994). In our structure, however, the indole ring of Trp50 is partially buried and approximately 7 Å from NAD at the nearest point. Thus, the crystal structure would suggest that Trp50 plays only an indirect role in NAD binding, possibly functioning as an anchor that stabilizes the loop containing Tyr54 (four residues away) which packs against the NMN ribose moiety of NAD.

DISCUSSION

Relevance of the Structure. The structure we have solved, whole DT (C-, T-, and R-domains) in complex with NAD, is not the biologically relevant species. The C-domain is the only portion of the toxin that is released into the cytoplasm where the ADP-ribosylation of EF-2 occurs. In fact, *in vitro* studies have shown that whole DT does not possess detectable ADP-RT activity toward EF-2 at all (Collier & Kandel, 1971). On the basis of the inactivity of whole DT, it is possible that there are significant structural differences between the isolated C-domain−NAD complex and the C-domain−NAD complex in the context of whole DT. However, there is much evidence suggesting that this is not the case. First, since the interface between the R-domain and the C-domain in whole DT is close to the active site of the C-domain (Choe et al., 1992; Bennett et al., 1994b; Bennett & Eisenberg, 1994), the inactivity of whole DT can be explained by the probability that the R-domain in whole DT blocks the entry of the diphthamide group of EF-2 into the active site of the C-domain. Second, NAD binds to whole DT and the isolated C-domain with nearly identical affinity (K_d = 8.6 and 8.3 μM for whole DT and the isolated C-domain, respectively; Lory et al., 1980; Kandel et al., 1974), suggesting that the NAD-binding sites are also identical. Indeed, in the structure of the whole DT−NAD complex described here, the R-domain makes no direct contacts to NAD, and thus the NAD-binding site in whole DT is located solely within the C-domain. This is in contrast to the DT−ApUp complex where Arg458 and Ser446 of the R-domain make direct contacts to ApUp. Finally, the crystal structures of the C-domain in the context of whole DT (both monomeric and dimeric) and in the isolated form are essentially identical in the active-site regions (Weiss et al., 1995).

On the basis of the assumption that the structure of the C-domain−NAD complex determined here in the context of whole DT is an accurate model for the structure of the isolated C-domain−NAD complex, we will address the following issues: (1) the mechanism by which the C-domain catalyzes the ADP-ribosylation of EF-2, (2) how the ADP-ribose acceptor substrate EF-2 is recognized by the C-domain−NAD binary complex, and (3) how NAD binds to other members of the ADP-RT family of enzymes based on structural alignment with the DT−NAD complex.

ADP-Ribosylation Mechanism. Two features of the structure of the DT−NAD complex stand out as being particularly relevant to the mechanism by which the C-domain catalyzes the ADP-ribosylation of EF-2: (1) the conformation of NAD when bound to the C-domain and (2) the proximity of the Glu148 carboxylate group of the C-domain to the scissile, N-glycosidic bond of NAD.

The conformation of NAD in the active site could be relevant to catalysis in two (nonmutually exclusive) ways. First, the C-domain binding to NAD could serve to expose and orient the C1′N atom for nucleophilic attack by the diphthamide imidazole group of EF-2 in an S_N2-type reaction as has been previously proposed (Wilson et al., 1990; Wilson & Collier, 1992). As viewed in Figure 4c, the C-domain binds to NAD such that the C1′N atom of NAD faces away from the active-site cleft and is exposed to solvent. In addition, the $\chi = 0°$ dihedral angle places the bulky part of the nicotinamide ring over the ribose ring, resulting in further exposure of the C1′N atom. In this way, the C-domain of DT would catalyze the ADP-ribosylation of EF-2, at least in part, by making the C1′N atom more susceptible to nucleophilic attack.

Second, the conformation of NAD imposed by the C-domain could place strain on the N-glycosidic bond, making NAD when bound to the C-domain less stable relative to an intermediate state in which the N-glycosidic bond is either elongated or broken. Whether or not the N-glycosidic bond is elongated in the complex is difficult to assess, as the degree of distortion would probably not be significant relative to the mean coordinate error at 2.3 Å

resolution. The highly folded, compact conformation of the NMN moiety of NAD in the complex with the C-domain results in some steric overlap which could potentially destabilize the N-glycosidic bond. In particular, the syn ($\chi = 0°$) conformation of the nicotinamide ring places O4′N of the NMN ribose and C2N of the nicotinamide ring in an eclipsed configuration. Thus, by imposing unfavorable nonbonded interactions on NAD in the complex, the C-domain could in part catalyze the ADP-ribosylation of EF-2 by (1) stabilizing (relative to the ground state) an oxocarbonium intermediate in which the nicotinamide ring has dissociated and/or (2) making nicotinamide a better leaving group in a nucleophilic displacement-type reaction.

The second feature of the DT−NAD complex that is most probably important for catalysis of the ADP-ribosylation reaction is the proximity of the Glu148 carboxylate group of NAD to the scissile, N-glycosidic bond of NAD. Previous studies, in which the γ-methylene carbon of Glu148 was UV cross-linked to the C6 atom of the nicotinamide ring of NAD, have identified the side chain of Glu148 as being near the nicotinamide portion of NAD in the complex (Carroll & Collier, 1984). Subsequent mutagenesis studies revealed that the carboxylate group of Glu148 is essential for catalysis of the ADP-ribosylation reaction (Wilson et al., 1990). A role for Glu148 in the reaction has been proposed in which the carboxylate group activates the diphthamide imidazole of EF-2 for a nucleophilic attack on C1′N, in an S_N2-type displacement reaction (Wilson et al., 1990; Wilson & Collier, 1992).

The crystal structure of the DT−NAD complex confirms that the side chain of Glu148 lies near the nicotinamide ring of NAD in the complex, as previously proposed: the γ-methylene carbon atom of Glu148 and C6 of the nicotinamide ring of NAD are 4.1 Å apart in the complex. In addition, the more precise definition of the geometry of the Glu148 carboxylate group relative to the N-glycosidic bond of NAD allows for a more accurate delineation of the possible role of this carboxylate group in catalyzing the ADP-ribosylation of EF-2. As seen in Figures 4b and 5, the Glu148 carboxylate group lies 4 Å from the positively charged N1N atom of the nicotinamide ring (forming a weak salt bridge) and 4 Å from C1′N. The observation that the negatively charged carboxylate group of Glu148 is within 4 Å of C1′N of NAD suggests that it could potentially stabilize a positively charged oxocarbonium intermediate in an S_N1-type mechanism, in which the nicotinamide ring has dissociated. If so, the inversion of configuration at C1′N (substrate is the β-anomer of NAD, product is the α-anomer of ADP-ribosyldiphthamide; Oppenheimer & Bodley, 1981) could be explained by the observation that NAD is bound by DT such that only the opposite side of C1′N (relative to nicotinamide) is exposed and able to react with the incoming diphthamide imidazole. In addition, the observation that the carboxylate group of Glu148 is only 4 Å from C1′N may place serious constraints on its ability to interact directly with the incoming imidazole group of diphthamide, as proposed for the S_N2-type mechanism.

Previous studies (Wilson & Collier, 1991) have suggested that His21, which lies in the active-site cleft near Glu148, may play a role in catalysis of the ADP-ribosylation reaction. This was based on the presence of a $pK_a = 6.2-6.3$ in the pH profile for the ADP-ribosylation reaction. The crystal structure of the DT−NAD complex, however, shows that His21 binds ∼7 Å from the N-glycosidic bond of NAD. Alternatively, His21 may play an important role in maintaining the integrity of the active-site pocket as it also hydrogen bonds to the backbone carbonyl of Tyr54, the side chain of which packs against the NMN ribose moiety of NAD (see Figure 4b). Indeed, mutational studies have shown that glutamine is the only acceptable substitution for His21 (Blanke et al., 1994a; Johnson & Nichols, 1994), indicating that both of these hydrogen bonds are essential for NAD binding.

EF-2 Recognition. Kinetic studies have shown that the transfer of an ADP-ribose group from NAD to EF-2 catalyzed by DT proceeds through an ordered, sequential mechanism, in which the C-domain first binds to NAD, forming a binary complex which then binds to EF-2 (Chung & Collier, 1977). Moreover, binding assays have shown that the C-domain binds to EF-2 only in the presence of NAD: when NAD is absent, there is no detectable interaction between the C-domain and EF-2 (Chung & Collier, 1977; Kessler & Galloway, 1992). It follows that (1) NAD binding induces some significant structural change in the C-domain which is important for binding to EF-2 and/or (2) NAD is bound to the C-domain such that some significant portion of NAD is exposed and important for binding to EF-2.

A major structural change that occurs in the C-domain upon NAD binding is in residues 39−46 of the active-site loop which become disordered. We observe that these residues are disorderd in each of the two molecules in the asymmetric unit of the DT−NAD crystal. Thus, we believe that this structural feature is inherent to the DT−NAD complex and not merely a consequence of crystal packing. Since this is the only significant structural change in the C-domain that is induced by NAD binding, it is probable that this loop is involved in binding to EF-2, as explained above. This loop may act as an arm which is dislodged from the C-domain structure after NAD binding and is then free to bind the acceptor substrate EF-2. This would explain (at least in part) why EF-2 is recognized by DT only after NAD has bound.

Two lines of biochemical evidence support this proposal. First, antibodies raised against a peptide corresponding to this loop sequence from residues 32 to 54 were able to block the C-domain of DT from catalyzing the ADP-ribosylation of EF-2 (Olson, 1993), suggesting that this loop has some essential function in the ADP-ribosylation of EF-2. Second, DT and ETA (ETA also catalyzes the ADP-ribosylation of EF-2) have a high degree of sequence similarity in this loop region, with identical or highly conserved substitutions at Lys37, Lys39, Ser40, Gln43, Asp47, and Trp50, which are Arg456, Arg458, Ser459, Gln460, Asp463, and Trp466 in ETA (Olson, 1993; Carrol & Collier, 1988). The high degree of sequence similarity between ETA and DT in these loop residues also suggests that they have some essential function. Since we have shown here that these residues are not involved directly in NAD binding, it is likely that this loop is necessary for binding to EF-2.

A second possible explanation for the dependence of the interaction between the C-domain and EF-2 on NAD is that some portion of NAD is exposed when bound to the C-domain and is important for binding to EF-2. As seen in the space-filling model of the DT−NAD binary complex shown in Figure 4c, the negatively charged phosphates and NMN ribose hydroxyls of NAD form an exposed surface which is not contacted by the C-domain. This surface provides the potential for electrostatic and hydrogen-bonding

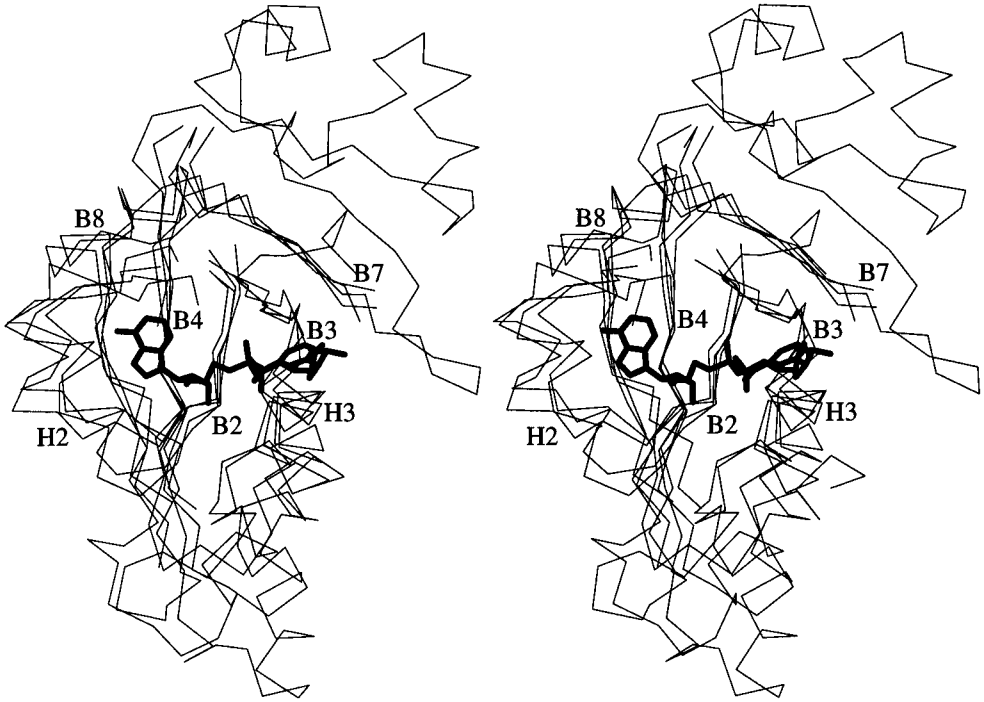

FIGURE 6: Stereoview showing the conserved ADP-ribosyltransferase (ADP-RT) NAD-binding fold that is common to four toxins. The catalytic domains of LT, PT, and ETA were aligned with the structure of the DT−NAD complex using only the Cα atoms and the algorithm of Kabsch (1978). Only those segments of PT, LT, and ETA that are common to each of the four ADP-RT enzymes are shown. These are residues 437−457, 469−505, and 552−573 of ETA, residues 4−25, 60−92, and 111−168 of LT, and residues 6−26, 51−96, and 127−148 of PT. Residues 18−187 of DT are shown. Each protein is represented as a Cα trace in thin lines, and NAD is shown in thick lines. The secondary structures of the aligned regions are labeled according to DT (see Figure 3). The coordinates for LT and PT were obtained from the Brookhaven Protein Data Bank (1LTS, 1PRT), and the coordinates for ETA were kindly sent to us by David B. McKay and David R. Davies.

interactions, points away from the active-site cleft of the C-domain, and thus appears to be presented for recognition by EF-2.

In summary, on the basis of the DT−NAD crystal structure, we propose that the C-domain−NAD binary complex binds to EF-2 through (1) the active-site loop residues 39−48 which become disordered upon NAD binding and (2) the negatively charged phosphates and NMN ribose of NAD which form an exposed surface when bound to the C-domain. This then provides a structural basis for the previously proposed sequential, ordered mechanism of ADP-ribosylation in which the C-domain binds first to NAD and then to EF-2. The dependence on NAD of the association between the C-domain and EF-2 could serve to prevent nonproductive interactions which may be critical for maximizing the efficiency with which the C-domain ADP-ribosylates EF-2 molecules within the cell and shuts down protein synthesis. This could be significant for allowing the high toxicity of DT even at minute concentrations.

NAD Binding to Other ADP-RT Enzymes. The structures of three other ADP-RT enzymes have been solved by X-ray crystallography. These are the catalytic domains of ETA (Allured et al., 1986), LT (Sixma et al., 1991), and PT (Stein et al., 1994). Like DT, ETA catalyzes the ADP-ribosylation of EF-2 at diphthamide, while LT and PT ADP-ribosylate the α-subunit of trimeric G-proteins at an arginine and a cysteine residue, respectively. While these four ADP-RT domains do not have a high degree of sequence identity (∼5−20%), they all have within them a common core fold of approximately 100 amino acids that contains the NAD-binding site. This common core fold consists of two antiparallel β-sheets and two α-helices, corresponding to CB8, CB4, CB2, CB3, CB7, CH2, and CH3 in DT (Figure 3). In each ADP-RT domain, a cleft is formed at the interface of the two β-sheets. On the basis of structural alignments with the DT−NAD complex, it should be possible to predict how NAD binds to each of these other ADP-RT enzymes. These modeling studies may be particularly useful since these other ADP-RT enzymes catalyze the hydrolysis of NAD (as does DT), making crystallographic binding studies difficult.

A superposition of the structures of the catalytic domains of ETA, LT, and PT aligned with the C-domain of the DT−NAD structure is shown in Figure 6, and a structure-based sequence alignment of the four enzymes is shown in Figure 7. A summary of the structural alignments, giving the information necessary to align the four structures, is presented in Table 4.

P. aeruginosa Exotoxin A. Residues 18−187 of DT and residues 437−585 of ETA can be aligned to a rms deviation of 2.1 Å for 117 pairs of Cα atoms. Although these enzymes have only 20% sequence identity in this aligned region, we find that all of the residues of DT which are in direct contact with NAD are strictly conserved in ETA. These are His21, Gly22, Thr23, Ser30, Ile31, Gly34, Phe53, Tyr54, Tyr65, Glu148, and Trp153 of DT, which are His440, Gly441, Thr442, Ser449, Ile450, Gly453, Phe469, Tyr470, Tyr481, Glu553, and Trp558 of ETA. Thus, the binding of NAD to ETA can be easily inferred from a comparison with the structure of the DT−NAD complex. ETA also has an active-site loop (residues 456−470) that is topologically identical to that of DT and binds to the same position over the active-site cleft. Arg458 of this loop overlaps with the predicted binding site of the adenosine ribose of NAD, suggesting a repositioning of this residue, and possibly the active-site loop,

```
                CB2          CH2
DT     18   SSYHGTKPGYVD.SIQK...GIQKP     38
ETA   437   VGYHGTFLEAAQ.SIVF..GGVRAR    458
PT      6   TVYRYDS..RPPEDVFQN..GFTAW     26
LT      4   RLYRADS..RPPDEI.KRSGGLMPR     25

                CB3   CH3                                  CB4
DT     53   FYSTDNKYDAA.GYS..VDNEN..PLS.........GK.AGGVVKVT.YPG    87
ETA   469   FYIAGDPALAY.GYA..QDQAPDARGR.........IR.NGALLRVY.VPR   505
PT     51   VSTSSSRRYTE.VYLEHRM..Q..EAVEAERAGRGTGHF.IGYIYEVR.AD.    94
LT     60   VSTSLSLRSAHLAGQSIL.....S...........GYSTYYIYVIATA..    91

                CB7          CB8
DT    146   SVEYINNWEQAKALSV.ELE.INF    167
ETA   551   RLETILGWPLAERTVV.IPSAIPT    573
PT    127   QSEYLAHRR.IPPENI.RRV.TRV    147
LT    110   EQEVSALGG.IPYSQIYGW..YRV    130
```

FIGURE 7: Sequence alignment of the ADP-ribosyltransferase core regions, based on a superposition of their structures. The ADP-RT core regions of ETA, LT, and PT (as defined in the legend to Figure 6) were each structurally aligned to that of DT using only the Cα atoms and the algorithm of Kabsch (1978). A sequence alignment was derived from each structural alignment. Residues of DT that contact NAD directly are indicated in boldface. Residues of ETA, LT, and PT that align near NAD of the DT−NAD complex, and thus are suggested to be involved in NAD binding, are also in boldface. The positions of the secondary structures in the sequence of DT are indicated by the solid lines and are labeled according to Figure 3.

Table 4: Structural Alignments of ADP-ribosyltransferase Enzymes with the C-Domain of DT[a]

enzyme	Cα atoms[b]	DT Cα atoms	rmsd	no. of Cα pairs[c]	rotation[d]			trans[e]
ETA	437−585	18−187	2.1	117	0.840	0.541	−0.046	−53.84
					0.352	−0.479	0.804	−38.81
					0.413	−0.692	−0.593	12.58
LT (1LTS)	4−130	18−167	2.6	82	−0.624	0.778	−0.073	−26.43
					−0.727	−0.612	−0.312	−28.28
					−0.287	−0.141	0.947	−52.51
PT (1PRT)	6−147	18−167	3.3	94	−0.303	−0.261	0.916	69.99
					−0.440	−0.815	−0.378	−27.66
					0.845	−0.518	0.132	4.56

[a] Structures were aligned using only Cα atoms and the algorithm of Kabsch (1978). [b] Cα atoms of the enzyme used to align with the C-domain of DT. [c] Number of pairs of Cα atoms included in the alignment. [d] Rotation matrix to be applied to enzyme coordinates to align with the C-domain of DT. [e] Translation vector (*x*, *y*, *z*) to be applied to the enzyme coordinates to align with the C-domain of DT.

upon NAD binding to ETA. Arg458 is close to the predicted phosphate-binding site and could potentially form a salt bridge with a phosphate in the ETA−NAD complex. Glu553 of ETA, a residue that has been shown to be essential for ADP-ribosylation catalysis (Douglas & Collier, 1987), aligns with Glu148 of DT. The carboxylate group of Glu553 of ETA superimposes almost exactly with that of Glu148 of DT and thus lies approximately 4 Å from the predicted position of the N-glycosidic bond of NAD.

E. coli Heat-Labile Enterotoxin. Residues 18−167 of DT and residues 4−130 of LT can be aligned to an rms deviation of 2.6 Å for 82 pairs of Cα atoms. Less than 10% (seven) of the aligned residue positions have identical amino acids, and only two of the residues of DT in direct contact with NAD (Gly34 and Glu148) are conserved in LT (Gly21 and Glu112). Thus, the precise mode of binding of NAD to LT cannot be directly inferred from the structure of the DT−NAD complex. An alignment of the DT−NAD complex with the LT structure (Figure 8) shows that the predicted NAD-binding site on LT overlaps with residues 48−56 of the active-site loop of LT, suggesting that these residues are displaced from the active-site cleft of LT upon NAD binding. This loop of LT is topologically similar to the active-site loop of DT that becomes disordered upon NAD binding. On the basis of this observation, it is interesting to speculate that this feature of an extended loop that is displaced from the active-site cleft upon NAD binding to a disordered state, and is involved in recognition of the ADP-ribose acceptor substrate (EF-2 in the case of DT and ETA, GS-α in the case of LT), is common to both DT and LT.

Assuming the displacement of residues 48−56 from the active-site cleft, possible interactions between residues of LT and NAD can be predicted on the basis of an alignment with the DT−NAD complex. Overall, NAD superimposes with a complementary groove on LT with the only steric overlaps occurring by the side chains of Arg11 and Asp9 of LT with the adenine ring and the adenosine ribose of NAD, respectively. This would suggest either a slight rearrangement of these side chains upon NAD binding or a slightly different positioning of the adenosine portion of NAD in the LT−NAD complex. The predicted adenine-binding site is also near the side chains of Ile16 and Leu22 of LT which form a hydrophobic pocket and is near the backbone C═O of Gly21 and NH of Met23. Arg7 of LT aligns with His21 of DT and could potentially bind to either the ribose or phosphate of the AMP portion of NAD. In the LT structure Arg7 hydrogen bonds to the backbone carbonyl of Ser61 and may play a similar role as His21 of DT in both NAD binding and maintenance of the active-site integrity, as has been proposed previously (Sixma et al., 1993). The predicted binding site for the NMN portion of NAD lies near the side chains of Ile76, Ala72, Glu110, Ser61, Glu112, and Ser63 of LT. The predicted position of the carboxamide group of the nicotinamide ring is near the backbone C═O and NH groups of Ala8. Glu112 of LT, a residue that has been shown to be essential for catalysis of the ADP-ribosylation reaction (Tsuji et al., 1990, 1991), aligns with Glu148 of DT. The carboxylate group of Glu112 of LT superimposes almost exactly with that of Glu148 of DT and thus lies approximately

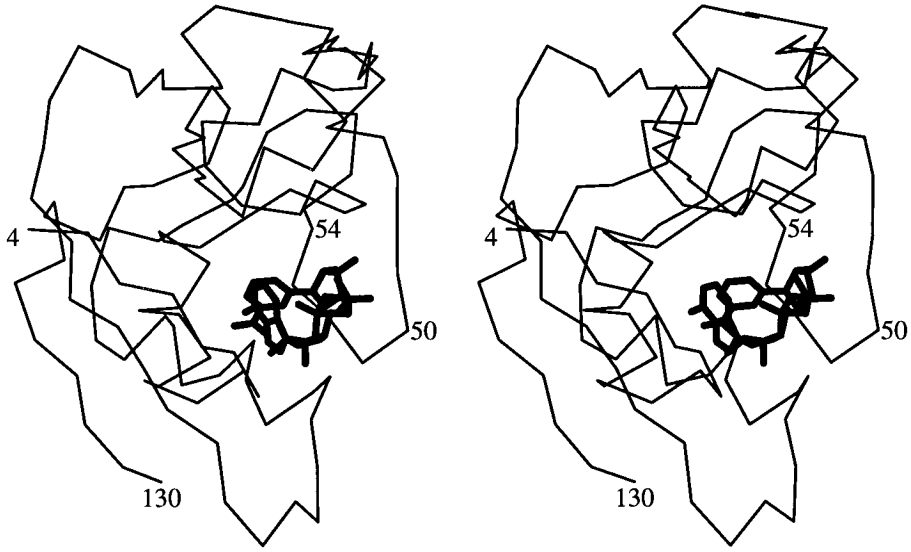

FIGURE 8: Stereoview showing the predicted NAD-binding site on the catalytic domain of *E. coli* heat-labile enterotoxin (LT) based on a structural alignment with the DT−NAD complex. The alignment of NAD with LT was based on residues 4−130 of LT and residues 18−187 of DT in complex with NAD. The protein atoms of DT are not shown. LT is represented as a Cα trace in thin lines, and NAD is shown in thick lines. Residues 4, 50, 54, and 130 of LT are labeled.

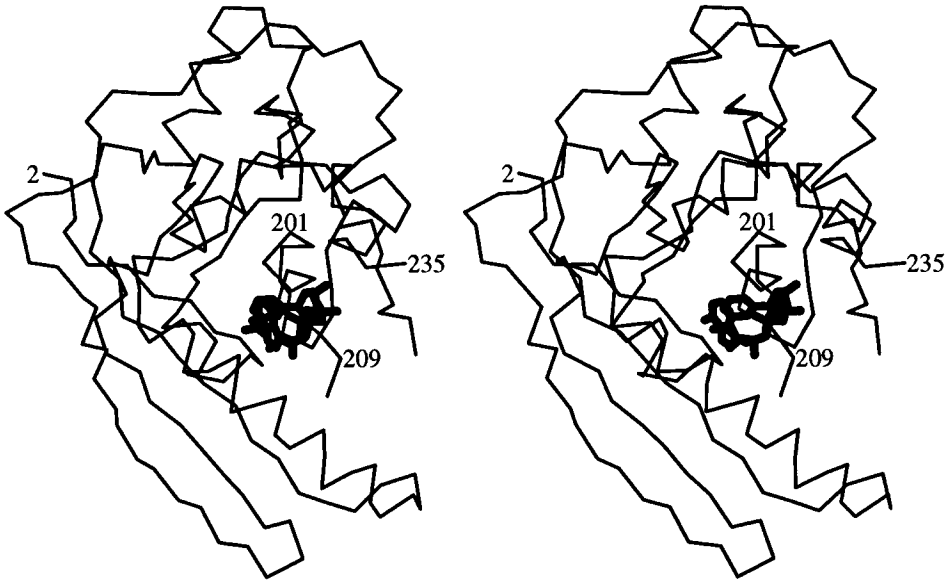

FIGURE 9: Stereoview showing the predicted NAD-binding site on the catalytic domain of pertussis toxin (PT) based on a structural alignment with the DT−NAD complex. The alignment of NAD with PT was based on residues 6−148 of PT and residues 18−187 of DT in complex with NAD. The protein atoms of DT are not shown. PT is represented as a Cα trace in thin lines, and NAD is shown in thick lines. Residues 2, 201, 209, and 235 of PT are labeled.

4 Å from the predicted position for the N-glycosidic bond of NAD.

Bordetella pertussis Toxin. Residues 18−167 of DT and residues 6−147 of PT can be aligned to an rms deviation of 3.3 Å for 94 pairs of Cα atoms. Less than 10% of the aligned residue positions have identical amino acids, and only two of the residues of DT in contact with NAD (Gly34 and Glu148) are conserved in PT (Gly22 and Glu129). The NAD-binding site on PT, predicted from an alignment with the DT−NAD complex (Figure 9), overlaps with residues 199−207 of PT which form a short helix. Cys201 of this helix forms a disulfide bridge with Cys41. Thus, an alignment of PT with the DT−NAD structure would suggest that reduction of the Cys201−Cys41 disulfide bond and displacement of the helix formed by residues 199−207 from the active site of PT would be required for NAD binding. These residues of PT, by analogy with the active-site loop of DT, could become disordered upon NAD binding and may be involved in binding to the ADP-ribose acceptor substrate GS-α.

Assuming the displacement of residues 199−207 of PT from the active-site cleft, possible interactions between residues of PT and NAD can be predicted on the basis of an alignment with the DT−NAD complex. The predicted adenine-binding site lies near the side chains of Val118, Phe23, Val51, and Trp26 of PT which form a hydrophobic pocket and also near the backbone C═O of Gly22 and NH of Thr24. The side chains of Arg13 and Asp11 of PT would bind near the adenine ring and adenosine ribose portions of NAD, respectively. Arg9 of PT aligns with His21 of DT and could interact with either the ribose or the phosphate of the AMP portion of NAD. The predicted nicotinamide-binding site lies near the side chains of Tyr63, Tyr59, Ser54, Glu129, Ser52, and Gln127 of PT. Tyr63 of PT aligns with Tyr65 of DT and could form a similar aromatic stacking interaction with the nicotinamide ring of NAD. The

predicted position of the carboxamide group of NAD would lie near the backbone C═O and NH groups of Tyr10. Glu129 of PT, a residue that has been shown to be essential for catalysis of the ADP-ribosylation reaction (Pizza et al., 1988; Cockle et al., 1989; Locht et al., 1989), aligns with Glu148 of DT. This places the carboxylate group of Glu129 approximately 4 Å from the predicted position of the N-glycosidic bond of NAD. Interestingly, the side chain of Gln127 of PT is also very near the predicted position of the N-glycosidic bond of NAD, suggesting a potential role for this residue in catalysis of the ADP-ribosylation reaction.

In summary, each of these four ADP-ribosyltransferase enzymes, DT, ETA, LT, and PT, contains a similar core NAD-binding fold. Alignments of ETA, LT, and PT with the DT−NAD complex reveal a structural element in each case, analogous to the active-site loop of DT, that could potentially be displaced upon NAD binding. In the case of LT and PT, removal of the active-site segment would appear to be required for NAD binding. It is tempting to suggest that each of these active-site segments plays a role in binding to the ADP-ribose acceptor substrate, as we argue is the case for the active-site loop of DT.

In addition, alignments of ETA, LT, and PT with the DT−NAD complex suggest common features of NAD binding for the ADP-RT family. Only two residues, Glu148 and Gly34 of DT, are strictly conserved in LT, PT, and ETA. The DT−NAD structure would suggest that the conserved glycine is important for main-chain hydrogen bonding to the adenine ring. The conserved glutamate residue aligns to the same position within the active-site cleft of each toxin and is likely to play a critical role in catalysis of the ADP-ribosylation reactions. Alignments with the DT−NAD structure would suggest that the carboxylate group of each of these glutamate residues binds ∼4 Å from the N-glycosidic bond of NAD in each of the toxin−NAD complexes. Each toxin also contains a residue (arginine in PT and LT; histidine in DT and ETA) that appears to be critical for both NAD binding and maintenance of the active-site integrity.

A genetically detoxified PT molecule has recently been developed for use as a new vaccine against whooping cough (Rappuoli et al., 1992a,b). It is interesting to note that this PT molecule contains the mutations Arg9 → Lys and Glu129 → Gly, identified above as being important residues for NAD binding and catalysis, respectively. This PT molecule was found to have significantly reduced toxicity and increased antigenicity when compared to other, chemically detoxified PT preparations used as vaccines. The crystal structure of the DT−NAD complex may be useful as a structural framework for developing genetically detoxified versions of other ADP-RT toxins, such as cholera toxin, for vaccination purposes.

ACKNOWLEDGMENT

We thank Dr. Duilio Cascio for help in data collection, Drs. Manfred S. Weiss, Melanie J. Bennett, Senyon Choe, and R. John Collier for useful discussions, and Drs. David B. McKay and David Davies for atomic coordinates.

REFERENCES

Allured, V. S., Collier, R. J., Carroll, S. F., & McKay, D. B. (1986) *Proc. Natl. Acad. Sci. U.S.A. 83*, 1320−1324.

Bennett, M. J., & Eisenberg, D. (1994) *Protein Sci. 3*, 1464−1475.

Bennett, M. J., Choe, S., & Eisenberg, D. (1994a) *Proc. Natl. Acad. Sci. U.S.A. 91*, 3127−3131.

Bennett, M. J., Choe, S., & Eisenberg, D. (1994b) *Protein Sci. 3*, 1444−1463.

Blanke, S. R., Huang, K., Wilson, B. A., Papini, E., Covacci, A., & Collier, R. J. (1994a) *Biochemistry 33*, 5155−5161.

Blanke, S. R., Huang, K., & Collier, R. J. (1994b) *Biochemistry 33*, 15494−15500.

Blewitt, M. G., Chung, L. A., & London, E. (1985) *Biochemistry 24*, 5458.

Brünger, A. T. (1990) *X-PLOR Manual Version 3.1*, Yale University, New Haven, CT.

Brünger, A. T. (1991) *Acta Crystallogr. A46*, 46−57.

Brünger, A. T. (1992) *Nature 355*, 472−474.

Brünger, A. T., Krukowski, A., & Erickson, J. (1990) *Acta Crystallogr. A46*, 585−593.

Burnette, W. N. (1994) *Structure 2*, 151−158.

Carroll, S. F., & Collier, R. J. (1984) *Proc. Natl. Acad. Sci. U.S.A. 81*, 3307−3311.

Carroll, S. F., & Collier, R. J. (1988) *Mol. Microbiol. 2* (2), 293−296.

Carroll, S. F., Barbieri, J. T., & Collier, R. J. (1986) *Methods Enzymol. 165*, 68−76.

Choe, S., Bennett, M. J., Fujii, G., Curmi, P. M. G., Kantardjieff, K. A., Collier, R. J., & Eisenberg, D. (1992) *Nature 357*, 216−222.

Chung, D. W., & Collier, R. J. (1977) *Biochim. Biophys. Acta 483*, 248−257.

Cockle, S. A. (1989) *FEBS Lett. 249*, 329−332.

Collier, R. J. (1975) *Bacteriol. Rev. 39*, 54−85.

Collier, R. J., & Kandel, J. (1971) *J. Biol. Chem. 246*, 1496−1503.

Collier, R. J., & Mekalanos, J. J. (1980) in *Multifunctional Proteins* (Bisswanger, H., & Schmincke-Ott, E., Eds.) pp 261−291, John Wiley & Sons, New York, NY.

Douglas, C. D., & Collier, R. J. (1987) *J. Bacteriol. 169*, 4967−4971.

Fujii, G., Choe, S., Bennett, M. J., & Eisenberg, D. (1991) *J. Mol. Biol. 222*, 861−864.

Hodel, A., Kim, S. H., & Brunger, A. T. (1992) *Acta Crystallogr. A48*, 851−858.

Johnson, V. G., & Nichols, P. J. (1994) *J. Biol. Chem. 269*, 4349−4354.

Jones, T. A. (1978) *J. Appl. Crystallogr. 11*, 268−272.

Kabsch, W. (1978) *Acta Crystallogr. 1734*, 827−828.

Kandel, J., Collier, R. J., & Chung, D. W. (1974) *J. Biol. Chem. 249*, 2088−2097.

Kessler, S. P., & Galloway, D. R. (1992) *J. Biol. Chem. 267*, 19107−19111.

Kraulis, P. J. (1991) *J. Appl. Crystallogr. 24*, 946−950.

Locht, C., Capiau, C., & Feron, C. (1989) *Proc. Natl. Acad. Sci. U.S.A. 86*, 3075−3079.

Lory, S., Carroll, S. F., Bernard, P. D., & Collier, R. J. (1980) *J. Biol. Chem. 255*, 12011−12015.

Morris, R. E., Gerstein, A. S., Bonventre, P. F., & Saelinger, C. B. (1985) *Infect. Immunol. 50*, 721−727.

Morris, A. L., MacArthur, M. W., Hutchinson, E. G., & Thornton, J. M. (1992) *Proteins 12*, 345−364.

Moskaug, J. O., Stenmark, H., & Olsnes, S. (1991) *J. Biol. Chem. 266*, 2652−2659.

Moss, J., & Vaughn, M. (1990) in *ADP-Ribosylating toxins and G proteins: Insights into signal transduction*, Library of Congress, Washington, DC.

Naglich, J. G., & Eidels, L. (1990) *Proc. Natl. Acad. Sci. U.S.A. 87*, 7250−7254.

Naglich, J. G., Metherall, J. E., Russell, D. W., & Eidels, L. (1992) *Cell 69*, 1051−1061.

Olson, J. C. (1993) *J. Bacteriol. 175*, 898−901.

Oppenheimer, N. J., & Bodley, J. W. (1981) *J. Biol. Chem. 256*, 8579−8581.

Papini, E., Schiavo, G., Sandona, D., Rappuoli, R., & Montecucco, C. (1989) *J. Biol. Chem. 264*, 12385−12388.

Papini, E., Santucci, A., Schiavo, G., Domenighini, M., Neri, P., Rappuoli, R., & Montecucco, C. (1991) *J. Biol. Chem. 266*, 2494−2498.

Passador, L., & Iglewski, W. (1994) *Methods Enzymol. 235*, 617−630.

Pizza, M., Bartoloni, A., Prugnola, A., Silvertri, S., & Rappuoli, R. (1988) *Proc. Natl. Acad. Sci. U.S.A. 85*, 7521−7525.

Rappuoli, R., Podda, A., Pizza, M., Covacci, A., Bartoloni, A., De Magistris, M. T., & Nencioni, L. (1992a) *Vaccine 10*, 1027−1032.

Rappuoli, R., Pizza, M., De Magistris, M. T., Podda, A., Bugnoli, M., Nanetti, R., & Nencioni, L. (1992b) *Immunobiology 184*, 230−239.

Rossmann, M. G., Liljas, A., Branden, C.-I., & Banaszak, L. J. (1975) *Enzymes 11*, 61−102.

Sandvig, K., & Olsnes, S. (1980) *J. Cell Biol. 87*, 828−832.

Sixma, T. K., Pronk, S. E., Kalk, K. H., Wartna, E. S., van Zanten, B. A. M., Witholt, B., & Hol, W. G. J. (1991) *Nature 355*, 561−564.

Sixma, T. K., Kalk, K. H., van Zanten, B. A. B., Dauter, Z., Kingma, J., Witholt, B., & Hol, W. G. J. (1993) *J. Mol. Biol. 230*, 890−918.

Slama, J. T., & Simmons, A. M. (1988) *Biochemistry 27*, 183−193.

Stein, P. E., Boodhoo, A., Armstrong, G. D., Cockle, S. A., Klein, M. H., & Read, R. J. (1994) *Structure 2*, 45−57.

Teng, T. Y. (1990) *J. Appl. Crystallogr. 23*, 387−391.

Tsuji, T., Inoue, T., Miyama, A., Okamoto, K., Honda, T., & Miwatani, T. (1990) *J. Biol. Chem. 265*, 22520−22525.

Tsuji, T., Inoue, T., Miyama, A., & Noda, M. (1991) *FEBS Lett. 291*, 319−321.

Van Ness, B. G., Howard, J. B., & Bodley, J. W. (1980) *J. Biol. Chem. 255*, 10710−10716.

Weiss, M. S., Blanke, S. R., Collier, R. J., & Eisenberg, D. (1995) *Biochemistry 34*, 773−781.

Wilson, B. A., & Collier, R. J. (1992) *Curr. Top. Microbiol. Immunol. 175*, 27−39.

Wilson, B. A., Reich, K. A., Weinstein, B. R., & Collier, R. J. (1990) *Biochemistry 29*, 8643−8651.

Wilson, B. A., Blanke, S. R., Reich, K. A., & Collier, R. J. (1994) *J. Biol. Chem. 269*, 23296−23301.

Yamaizumi, M., Mekada, E., Uchida, T., & Okada, Y. (1978) *Cell 15*, 245−250.

BI9520848